ACS NANO

www.acsnano.org

ARTICLE

Giant Second Harmonic Generation Enhancement in a High-*Q* Doubly Resonant Hybrid Plasmon–Fiber Cavity System

Qi Ai,* Florian Sterl, Han Zhang, Jianfang Wang, and Harald Giessen*

Cite This: *ACS Nano* 2021, 15, 19409–19417

Read Online

ACCESS | Metrics & More | Article Recommendations | Supporting Information

ABSTRACT: A high-quality plasmon–fiber cavity in a doubly resonant configuration can exhibit second-harmonic generation (SHG) with over 5 orders of magnitude enhancement compared to gold nanoparticles on a fused silica substrate. Through coupling to a fiber cavity with the proper diameter, a high-quality ($Q \approx 160$) resonance can be achieved in combination with a single gold nanoparticle. In a classical picture, where the incident electric field travels coherently Q times around the fiber during the nonlinear process, the high Q of the coupled mode aids in highly efficient SHG. We accomplish two feats: First, we analyze the Q factor dependence of the SHG efficiency, proving the expected Q^4 dependence and thus confirming coherent E-field amplification in the fiber cavity. Second, we carefully adjust the fiber size further and tune the plasmon response of a gold nanoparticle to a high-Q cavity mode. We make sure that the second harmonic wavelength is simultaneously in resonance with a higher order fiber cavity mode, fulfilling the *doubly resonant* condition. As a result, a giant SH response with conversion efficiency up to 1.6×10^{-5} is detected upon a pump intensity of 5×10^8 W/cm^2 for 100 fs pump pulses around 840 nm incident wavelength. Additionally, the importance of the doubly resonant condition is proven by detuning the size of the fiber, which leads to a drastic drop in SHG efficiency. This disparity of the SHG efficiency can be observed even by eye, when monitoring the intensity changes of the visible SH light during detuning.

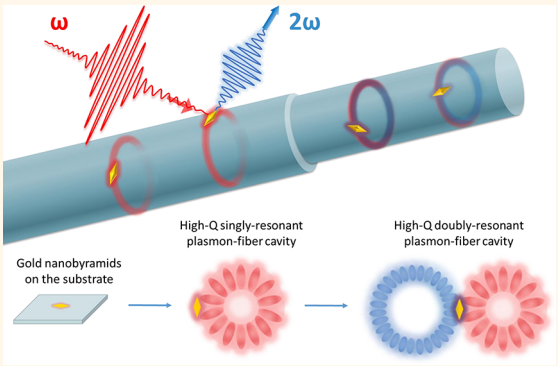

KEYWORDS: *nonlinear plasmonics, second-harmonic generation, multiple resonance plasmonics, high quality factor, microcavity*

Metals were not considered as suitable material for nonlinear optics research or applications for a long time because of their low optical nonlinearities. The second order nonlinear effect in particular is forbidden in most metals because of their inversion centrosymmetric structures. However, a second-harmonic (SH) response at a Ag–air interface was reported in 1974.[1] It was found that nonlinear polarization in metals can be induced by surface plasmon polaritons at the symmetry-breaking metal–air interface. Afterward, as nanofabrication techniques advanced and the ability of probing optical fields at the nanoscale improved,[2,3] metallic nanostructures that support localized surface plasmon resonances showed great potential to leverage nonlinear effects by confining the incident light into a nanoscale volume.[4−12]

In recent years, a great deal of effort has been put into promoting the nonlinear conversion efficiency, especially the SH conversion efficiency of metallic nanostructures, for example, by combining nanostructures with highly nonlinear materials,[13−16] designing special non-centrosymmetric structures[17−19] or toroidal-resonant plasmonic metasurfaces,[20] utilizing the interaction between localized and delocalized plasmons,[21,22] coupling plasmonic modes to electronic intersubband transitions in semiconductor heterostructures,[23] etc. However, the origin of second harmonic generation (SHG) and the fundamental mechanism of SH enhancement effects in metallic nanostructures are still under debate. Especially, some unexpected observations emerged when researchers were trying to enhance the SH responses based on the preconceived designs. For example, breaking of the centrosymmetry does not induce an increasing SH intensity in coupled plasmonic nanoparticles compared to symmetric systems.[24] Furthermore, fewer particles in a cluster can exhibit an even more efficient

Received: July 14, 2021
Accepted: November 30, 2021
Published: December 6, 2021

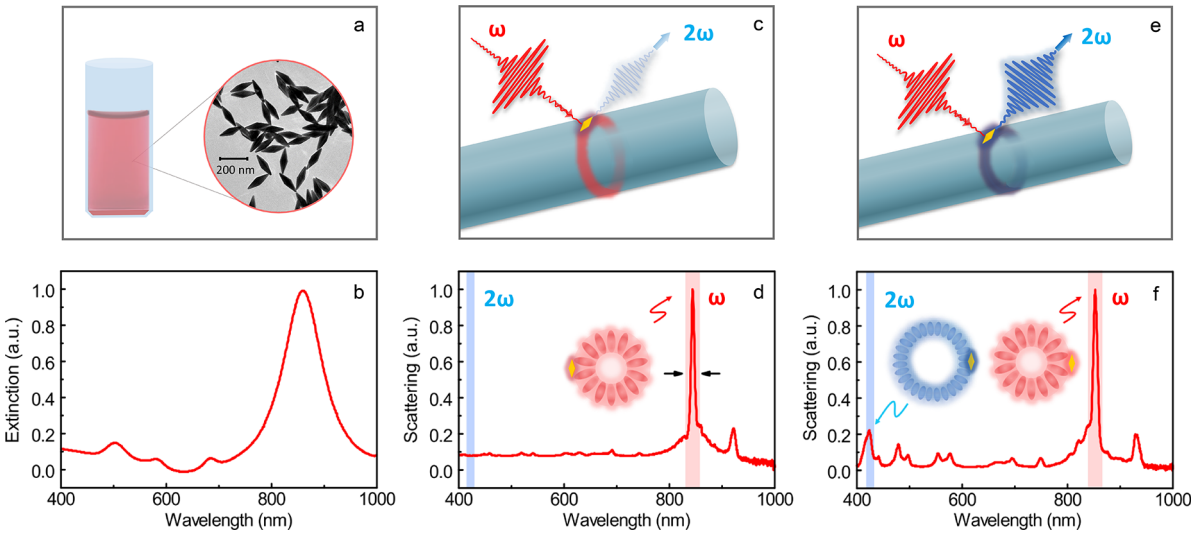

Figure 1. Design idea and working principle of the doubly resonant plasmon−fiber cavities. (a) Sketch and TEM image of gold nanobipyramids in solution. (b) Typical measured extinction spectrum of the sample shown in panel a. (c) Sketch of a singly resonant hybrid plasmon−fiber cavity. (d) Typical measured scattering spectrum and schematic electric field profile of a hybrid system as shown in panel c. (e) Sketch of a doubly resonant hybrid plasmon−fiber cavity. (f) Typical measured scattering spectrum and schematic electric field profiles at both fundamental and SH wavelength of a doubly resonant plasmon−fiber cavity as shown in panel e.

SH response.[25] Despite these unclear effects, it is evident that a resonance at the fundamental frequency and its quality are crucial for all harmonic generation processes. This fact is confirmed by the anharmonic oscillator model that has been well utilized to predict harmonic signals.[26,27] Nevertheless, systematic *Q*-dependent measurements were still lacking.

Recently, multiresonant plasmonic structures have been investigated and have attracted much attention, due to their potential for augmenting SHG.[28−31] These structures are composed of several plasmonic building blocks whose elementary plasmonic modes strongly interact with each other. Thus, multiple hybridized modes are generated and can be designed to be resonant at both the fundamental and the second harmonic frequencies. In this case, the input and signal fields of nonlinear origin are enhanced simultaneously. These enhancement mechanisms have also been demonstrated experimentally.[32] However, due to the large damping losses of the metallic structures, the near-field enhancement of those multiple resonant systems is still limited.

In fact, dramatically more efficient nonlinear responses in doubly resonant systems can be expected, when considering that the quality factor of the resonances can be drastically improved by designing special coupled systems. For example, relatively high quality factors of up to 100 can be achieved by arranging metal nanoparticles into periodic arrays.[33,34] A series of studies proved that the light−matter interaction is indeed enhanced in those high-*Q* plasmon systems.[26,35−37] Very recently, the nonlinear responses of multiresonances with high *Q* factors in an array of L-shaped aluminum nanoparticles has been numerically investigated.[38] Over one-million-fold enhancement of the emitted SH intensity with a conversion efficiency of 10^{-5} has been predicted when compared to an individual particle.

In this work, we demonstrate a high-*Q* doubly resonant plasmon−fiber system to greatly boost the second harmonic response through the coupling between the plasmon modes and optical modes in the microfiber cavity. Light can be confined within the fiber cavities by continuous total internal reflection, known as whispering gallery mode (WGM), and the fiber size can be easily modified by flame-heated pulling. It is a desired and operable method to enhance the interaction between the light and metallic particles by coupling the gold nanoparticles to the microfibers. A high-*Q* multiresonant coupled system can be achieved when nanoparticles are deposited onto the surface of microfibers with the proper diameter. Thanks to the simultaneous realization of high quality and the doubly resonant case, the second harmonic generation is successively enhanced by 5−6 orders of magnitude. This brings nonlinear plasmonics much closer toward real applications in nonlinear optical elements at the nanoscale. Plasmon−fiber cavities are also widely applied in a variety of sensors with high sensitivity.[39−41] Our work has huge potential to develop nonlinear plasmon sensing with even larger sensitivity based on the nonlinear conversion process.

RESULTS AND DISCUSSION

Working Principle of the Doubly Resonant Plasmon−Fiber Cavities. The idea of promoting the second harmonic conversion efficiency in hybrid plasmon−fiber cavities is illustrated in Figure 1. It mainly includes two steps: The first step is to coat the nanoparticles onto the surface of tapered microfibers (see Figure 1c)[42] to realize efficient coupling between the plasmon resonance and the WGMs. When illuminated, the gold nanoparticle on the fiber surface acts as an antenna interacting with the incident light, while the tapered fiber acts as an optical microcavity that confines the light at resonant frequencies, extends the interaction time, and fundamentally alters the interaction between the light and the gold nanoparticle. Thus, a high-*Q* resonance with a large field enhancement can be achieved (see Figure 1d). The second step is to decrease the diameter of the microfibers in our hybrid system to observe higher-order cavity modes. We then tuned one mode resonantly to the SH wavelength by carefully adjusting the size of the tapered fibers (see Figure 1e). In contrast to former multiresonant systems, in which the second resonance matched to the SH wavelength is just another

https://doi.org/10.1021/acsnano.1c05970
ACS Nano 2021, 15, 19409−19417

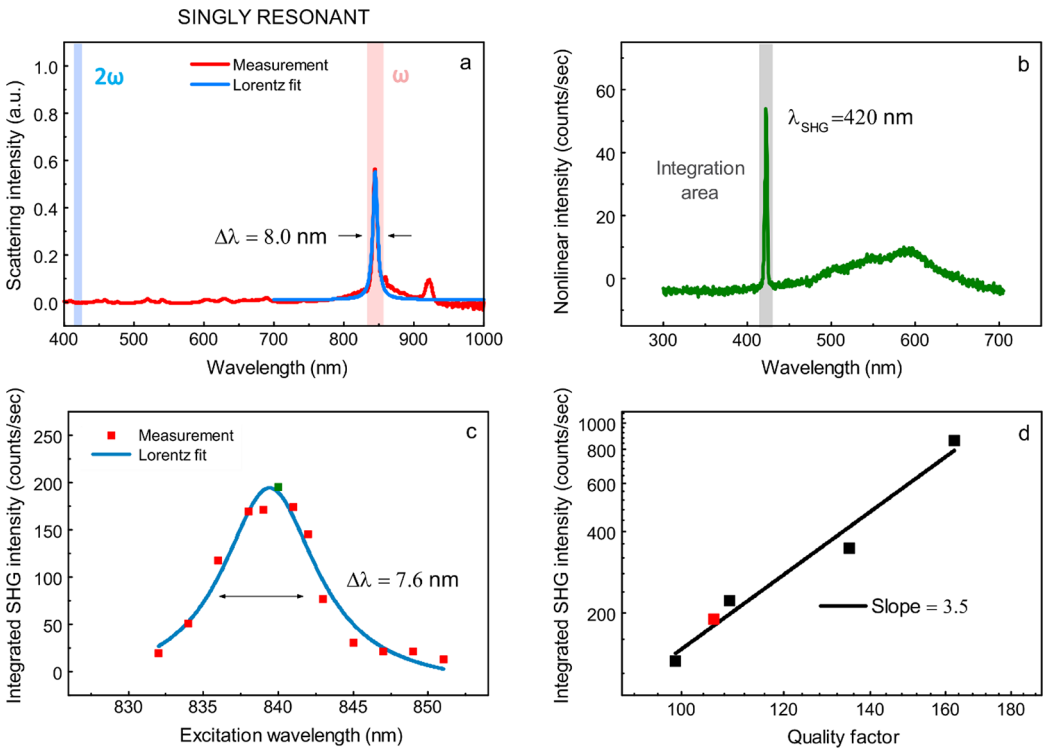

Figure 2. Linear and nonlinear responses from a *singly* resonant plasmon−fiber cavity and *Q*-dependent SHG. (a) Measured scattering spectrum (red, measurement; blue, Lorentz fit) of a single gold nano-bipyramid on a tapered fiber surface in the singly resonant case. (b) Nonlinear emission spectrum at the excitation wavelength matched to the central wavelength of the linear scattering resonance in panel a. (c) Corresponding SHG efficiency as a function of excitation laser wavelength (squares, measurement; blue curve, Lorentz fit). The single green square corresponds to the nonlinear emission spectrum in panel b. (d) Double-log plot of the *Q*-dependence of the SHG intensity. Five squares represent five singly resonant plasmon−fiber cavities with different *Q* factors. The single red square corresponds to the plasmon−fiber cavity shown in panels a−c. Linear and nonlinear responses of other plasmon−fiber cavities corresponding to the four black squares are shown in Figure S3.

hybrid plasmon mode, the second mode in our hybrid system arises from the coupling between the nanoantenna and the optical cavity. In this case, both the fundamental and the SH light circulate and interact dozens of times in a coherent fashion inside the microcavity. This leads to high-*Q* resonances with a strongly enhanced response in both linear and nonlinear regimes (see Figure 1f). As a result, giant SHG can be achieved by enhancing the quality factor and tuning the system into the doubly resonant condition.

In general, gold nanoparticles in aqueous solution or on fused silica substrates feature only a weak plasmon resonance with a low quality factor mainly due to the large damping losses of the metallic nanoparticles. Compared to the gold nanorods deposited on a tapered fiber surface that were investigated in our former work, the gold nano-bipyramid (NBP)-coupled system enables a higher conversion efficiency of the second-harmonic response. We believe that there are two reasons: On the one hand, the sharper tips of the gold nano-bipyramids produce stronger near-field localization. On the other hand, narrower localized surface plasmon resonances (LSPRs), which correspond to longer plasmon lifetime, can be achieved in gold nano-bipyramids.[43] Thus, the longer interaction time between longitudinal surface plasmon resonances of gold NBPs and WGMs of microfibers will lead to stronger interaction. In the experiment, when comparing dozens of gold nanorods with gold nano-bipyramids, we found indeed that we need substantially lower input powers in order to obtain similar or even much larger nonlinear signals when switching to gold nano-bipyramids. Single-crystalline gold nano-bipyramids that are used in this work were synthesized using an optimized seed-mediated growth method, which is introduced in the Methods section in detail. High-purity NBPs with desired longitudinal surface plasmon resonances can be grown by modifying various parameters in the growth solution. Synthesis details are described in the Methods section. A transmission electron microscopy (TEM) image of the gold nano-bipyramids is displayed in the inset of Figure 1a. Figure 1b displays the UV−vis spectrum of the corresponding NBPs in aqueous solution. More details including the finite-difference time-domain (FDTD) simulated extinction spectrum can be found in ref S4. Corresponding to the central wavelength (λ), 937 nm, and the resonance line width ($\Delta\lambda$) around 100 nm, the *Q*-factor ($\lambda/\Delta\lambda$) is less than 10. When the NBPs are coated onto a fused silica substrate, the central wavelength of the individual particles will blue shift to around 860 nm (see Figure S1) due to the change of refractive index of the surrounding media. The full width at half-maximum (FWHM) of the scattering spectrum is still broad around 100 nm (see Figure S1).

The microfibers used in our coupled system are manufactured by tapering single-mode fibers with a home-built flame-heated pulling machine,[44] which enables precise tailoring of the diameter of the tapered fibers as well as their waist length. By drop coating properly diluted gold NBPs onto the microfibers and letting them dry in ambient air, we can create hybrid plasmon−fiber cavities. When the diameters of fibers

https://doi.org/10.1021/acsnano.1c05970
ACS Nano 2021, 15, 19409−19417

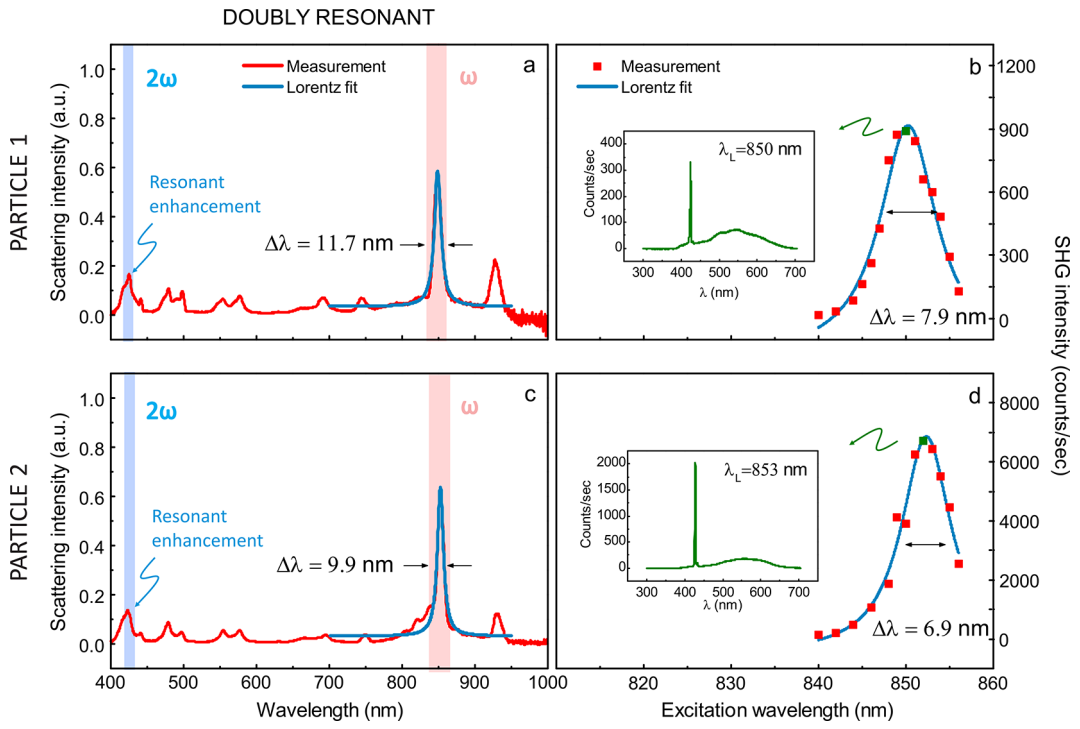

Figure 3. Linear and nonlinear response for two different particles (upper and lower row) from the *doubly* resonant plasmon−fiber cavities. (a, c) Scattering spectra (red, measurement; blue, Lorentz fit) from two gold bipyramids coupled to the same microfiber with diameter about 1.4 μm; (b, d) the corresponding SHG efficiency as a function of excitation laser wavelength (squares, measurement; blue curves, Lorentz fit). In panels b and d, nonlinear emission spectra at peak wavelength of SHG resonance are shown in the inset (green curves). The FWHM line widths, $\Delta\lambda$, of the linear and the second-harmonic resonances are marked in panels a−d.

are smaller than 2 μm, the radiation losses increase quickly.[45] In this case, the plasmon resonances of attached gold nanoparticles can efficiently couple to WGMs of microfibers via the strong evanescent field. Due to the large interparticle distance, no dipole−dipole coupling between two gold nanoparticles occurs. When gold NBPs are deposited on a microfiber with a diameter around 1.65 μm (see Figure 1c), a very narrow hybrid plasmon−fiber resonance with high Q factor of up to 160 is detected (see Figure 1d). In fact, the diameter of 1.65 μm is the proper fiber size to obtain the narrowest hybrid resonance, which was substantiated by a series of experiments. As the diameter of the fiber continues to decrease, the coupling with the light at the fundamental wavelength gets weaker, while some larger frequency modes arise. These modes exhibit weaker coupling, as displayed by the peak with the blue-striped background in Figure 1f. By carefully tuning the fiber diameter to 1.44 μm, this peak is matched to the SH wavelength, corresponding to the fundamental wavelength (as displayed by the peak with the red-striped background in Figure 1f). In this case, the quality factor turns out to be smaller due to weaker coupling but is still as high as 100. More details will be discussed later with regards to Figure 3.

Quality-Factor-Dependent Second Harmonic Response. The attractive properties of this fiber-coupled system are not only the enhanced optical response but also the tunable Q factors. Previous studies have already indicated that a resonance at the fundamental frequency and its quality are crucial for higher harmonic generation.[26,46−48] Here, we analyze carefully the relationship between the SH intensity and the system quality.

The coupling strength and thus the quality factor in our hybrid system are mainly determined by the size of the gold NBPs and the diameters of the microfibers. Meanwhile, they also depend on the different orientation of the particles lying on the fiber surface. This property was nicely demonstrated by Wang et al.[45] The tapered fibers have a waist-like shape, which means that the cavity size changes slightly at different positions on the fiber surface. Those properties enable us to study the hybrid systems with different Q factors as expected. It is worth mentioning that the incident angle influences both the wavelength position and the line width of the hybrid resonance.[42] Thus, the excitation conditions including the incident angle and the focus case are kept the same during the entire measurement process demonstrated in this work.

In order to detect the linear scattering resonance from the hybrid system without strong scattering from the bare fiber surface, a side-illumination method is used (see Figure S2). A dark-field scattering microscopy setup was utilized to perform linear and nonlinear spectroscopy. With this setup, the white light in the linear response measurement and the laser source in the nonlinear response measurement can be easily switched while maintaining the same incident condition. Figure 2a depicts the scattering spectrum of a single gold NBP displayed in Figure 1a coated on the microfiber with a diameter of 1.65 μm. The FWHM of its Lorentz fitting resonance (blue curve in Figure 2a) is 8 nm, which corresponds to a high Q factor of 105. When efficient coupling between the plasmon resonance of the gold NBP and the cavity mode resonant at 840 nm occurs, other cavity modes are barely coupled to the plasmonic particle, and thus no photons at other frequencies are radiated from the plasmonic antenna. Next, the sample was illuminated by the laser and its nonlinear response spectrum was detected

https://doi.org/10.1021/acsnano.1c05970
ACS Nano 2021, 15, 19409−19417

(see Figure 2b). A narrow SHG peak and broad photoluminescence (PL) are both observable. The analysis of the photoluminescence in this system was reported in our recent work.[49] By tuning the central wavelength of the excitation laser over the linear resonance step by step, we obtained a series of nonlinear emission spectra. For each spectrum, we determined the integrated SHG area by taking the overall SHG intensity minus the PL values. After plotting them as a function of excitation wavelength, we observed that the nonlinear spectroscopy gave rise to a narrow second-harmonic resonance as shown in Figure 2c. The single green square corresponds to the SHG peak intensity of the nonlinear spectrum in Figure 2b.

The line width, $\Delta\omega$, of the linear resonance plays a key role in the nonlinear yield, as has been shown by an anharmonic oscillator model.[26] Combined with the fact that the second-order nonlinear polarization scales quadratically with the fundamental field intensity, the anharmonic oscillator model predicts that the nonlinear efficiency of SHG scales to $1/\Delta\omega^4$.[26] In order to investigate this power dependence, we measured five hybrid systems with different Q-factors as displayed in Figure 2d. The actual measured linear and corresponding nonlinear scattering spectra are plotted in Figure S3. The FWHM of the linear scattering spectra in Figure S3a−e varies from 8.4 to 5.1 nm, which are all smaller than that of the excitation pulse (~10 nm), and their corresponding Q-factors range from 98 to 165. Therefore, the condition of infinite Q does not apply here.[50] Their corresponding SH resonances are displayed in Figure S3f−j. The green curves in the insets of Figure S3f−j are the nonlinear response spectra corresponding to the green squares in the SH resonances, which are the case when the laser excitation is at the peak wavelength of the linear resonance. The line width of the SHG peak ranges between half the linear resonance line width and half the laser spectral width. Meanwhile, as the line width of the linear resonance decreases, corresponding to a bigger Q-factor, the SH resonance turns out to be narrower than expected, while the SHG intensity increases. In order to investigate the Q-dependent SHG behavior, we plotted the peak intensity of the SH resonance of those five systems as a function of their system quality factors on a double-log plot and fit them by a linear function, as depicted in Figure 2d. The results clearly demonstrate the Q^4 dependence of SHG efficiency as predicted.[26] The SHG peak intensity of the system with a Q factor of 165, as displayed in Figure S3e,j is enhanced by more than 1 order of magnitude compared to the system with a Q factor of 95 as seen in Figure S3a,f.

Doubly Resonant Plasmon−Fiber Cavities. As mentioned before, 1.65 μm is the proper fiber size to couple to the gold NBPs used in this work. The electromagnetic energy of certain frequencies perfectly matches the modes of this whispering gallery without too much energy leakage. As the diameter of the tapered fiber decreases, higher-order cavity modes appear. By fine-tuning the fiber diameter to 1.44 μm, we obtain a *doubly* resonant system as displayed for two different particles in Figure 3a,c. The FWHM values of those two typical systems are 11.7 and 9.9 nm, respectively. The corresponding Q factors are 73 and 86, respectively, which are somewhat smaller than the perfect coupling systems as depicted in Figure 2 and Figure S3. On the other hand, the higher modes overlap with the SHG spectral position of the laser (indicated by the blue vertical stripes). By sweeping the laser wavelength over the linear resonance range, we obtain a series of nonlinear emission spectra, and typical ones are plotted as the insets of Figure 3b,d as green curves. After plotting the SHG peak intensity as a function of excitation wavelength, we found that nonlinear spectroscopy revealed narrow second-harmonic resonances of those two systems. By comparison of the doubly resonant system (see Figure 3d, normalized to the same incident power and exposure time) to the singly resonant system (see Figure S3b), the SHG peak intensity exhibits over *50-fold enhancement* even though the Q-factor is slightly smaller. Simultaneously, the line widths of the SH resonances of doubly resonant systems are narrower than those of singly resonant systems with equal Q-factors. This proves once more that the doubly resonant case enhances the nonlinear response by matching the SH light inside of the optical fiber cavities.

Nonlinear Response Comparison between Isolated Gold NBPs on the Substrate and Singly and Doubly Resonant Plasmon−Fiber Cavities. In order to confirm the huge SHG enhancement effect from our tailored high-Q doubly resonant systems further, we compared the nonlinear emission spectra from typical doubly and singly resonant systems with individual gold NBPs on a fused silica substrate. The excitation conditions and spectroscopy processes remained exactly the same during this comparison. By comparing Figure 4a,b, we clearly find that the SHG peak is orders of magnitude enhanced in the doubly resonant case while the intensities of the fundamental peaks are at a similar level. This proves that the second harmonic conversion efficiency is indeed drastically boosted in the doubly resonant case. As reference, the nonlinear emission spectrum of a single gold NBP on the fused silica substrate is displayed in Figure 4c. As mentioned, the plasmon resonance of the single gold particles is quite weak due to the large damping losses (see Figure S1). Hence, the fundamental scattered laser peak in the spectrum shown in Figure 4c is also quite weak compared to those in the fiber-coupled systems as displayed in Figure 4a,b. The nonlinear response spectrum with its SHG peak in the bottom left of Figure 4c is magnified by a factor of 1000 in that plot. The exposure time of the detector was 20 min, because the signal was quite weak. In fact, the SHG peaks in most cases cannot even be detected with that excitation power (160 mW) and an exposure time of 20 min. The nonlinear response from the particles also depends on their orientations on the substrate under side-illumination conditions. With a fixed incidence angle and s-polarization, particles with different orientations on the substrate possess different phase matching conditions with respect to the excitation light. Considering the weak nonlinear response, a set of measurements for the particles on a substrate have been carried out. Typical spectra are displayed in Figure S4. Comparing the intensity of SHG peaks in the nonlinear emission spectra of the doubly resonant system (around 6000 counts per second, see Figure 4a) with a particle on the substrate (0.055 counts per second, see Figure 4c), over 5 orders of magnitude enhancement is achieved. Photographic snapshots of the second-harmonic images of the particles are displayed as insets of Figure 4a,b and have been taken with an Allied Vision GC2450c CCD camera behind a short-pass filter and connected to our dark-field reflection setup as imaging component (see Figure S2). The observed green color is created by the wavelength-dependent camera efficiency. A movie that records the dynamic nonlinear light from the gold NBPs on the tapered fiber with diameter 1.44 μm when the focus area of our excitation laser sweeps from left to right over the tapered fiber and then turns back is included

https://doi.org/10.1021/acsnano.1c05970
ACS Nano 2021, 15, 19409−19417

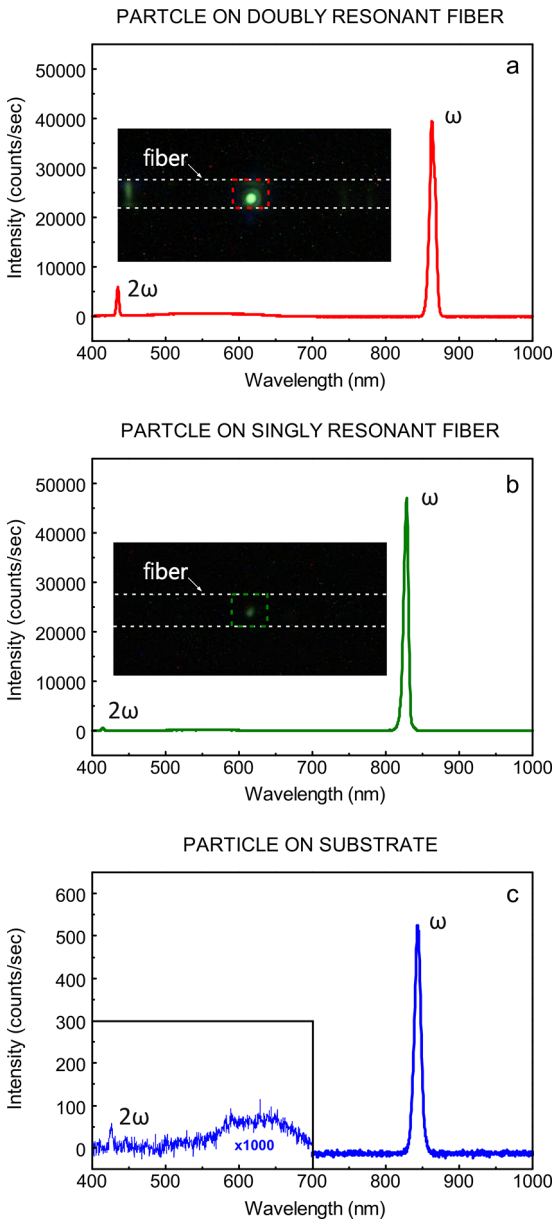

Figure 4. Nonlinear response comparison among single gold NBPs on the substrate and singly and doubly resonant plasmon−fiber cavities. (a) Spectrum indicating the fundamental and the SHG light for the doubly resonant plasmon−fiber cavities. (b) Spectrum indicating the fundamental and the SHG light for the singly resonant plasmon−fiber cavities. Insets in panels a and b depict the fiber−particle image, displaying the SH light, recorded with a camera. (c) Spectrum showing the fundamental and the SHG light for the particle on the substrate. The intensity of the left-bottom spectrum is magnified 1000 times.

as a Supplementary Movie. It was taken with a smartphone camera through the eyepiece of the microscope.

In order to quantify the real intensity of the SH response, we used an indirect method to measure and calculate it, which is described in Methods and the Supporting Information. A similar method to estimate the SH output power was also utilized by other groups.[25] Conversion between the intensity and the counts measured by the spectrometer can be performed throughout the entire wavelength range. By assuming that almost all the SHG is emitted toward the objective side and collected by the objective and by considering the losses due to the transmittance of the objective (~85%) together with the short-pass filter (~87%) in the collection path at the SH wavelength, we obtained a SHG peak power of ~0.28 μW, corresponding to 6000 counts/s shown as the blue square in Figure S5. By considering the spot size of the excitation laser beam impinging onto the sample (an oval area with long axis ~800 μm and short axis ~100 μm) and an absorption cross-section of 56000 nm^2 of the isolated particle, we estimated a SH conversion efficiency of $P_{SH}/P_F \cong 1.6 \times 10^{-5}$, where P_{SH} and P_F are the estimated average power for the SHG emission and the fundamental wavelength illumination, respectively (Table S1). This metric is commonly used in the case that the area of the nanostructure is much smaller than the excitation spot.[51] Our maximum employed incident power (~160 mW) yields 5×10^8 W/cm^2 pump intensity,[30] which is well below the experimental nanoparticle damage threshold[13,21] in our hybrid systems. It was also verified that we had stable SHG signals with the expected quadratic dependence on input power (see Figure S5). Compared to the doubly resonant plasmonic nanoantennas with low Q factor, we have almost *4 orders of magnitude* higher SH conversion efficiency. By comparison of the coupled gold nano-bipyramids and gold nano-bipyramids on a bare substrate, our calculated SHG peak intensity confirms the extraordinarily strong SHG enhancement in our high-Q doubly resonant plasmonic system.

CONCLUSION

In summary, we have presented a multiresonant high-Q plasmonic system based on efficient and tailored coupling between gold nano-bipyramids and tapered microfibers. Excellent plasmonic properties in the linear as well as the nonlinear regime have been demonstrated experimentally. In particular, the giant SHG intensity represents a record of nonlinear SHG conversion efficiency from single plasmonic nanoparticles. In our system, it is highly challenging to obtain exact quantitative conversion efficiencies due to the large size mismatch between our plasmonic system and the laser spot. By carefully design and material engineering with optimized parameters, similar structures such as metasurfaces based on the same working principle could be realized to precisely evaluate the resulting SHG power and its conversion efficiency. Relying on more flexible parameters, even more efficient coupling strength and higher SHG power could be expected in high-Q doubly resonant metasurfaces.[38] In addition, some other material that could sustain high temperatures, for example, titanium nitride,[52] could be considered to be used to boost the nonlinear process further with higher excitation power. For applications, our system with ultranarrow SH resonances and giant SHG peak intensities is a promising structure to realize nonlinear hydrogen sensing by replacing gold nanoparticles with palladium-capped gold nanoparticles in the future. Furthermore, fiber-coupled nanostructures with a high nonlinear conversion efficiency offer appealing opportunities for the development of nonlinear optics-based single-photon sources.

METHODS

Sample Preparation. *Preparation of the Au Nano-bipyramids.* The Au nano-bipyramids (NBPs) were grown using a seed-mediated growth method, as reported in previous works.[53−55] Specifically, the seed solution was prepared by adding a freshly prepared, ice-cold $NaBH_4$ solution (150 μL, 0.01 M) into an aqueous solution composed of DI water (9.625 mL), $HAuCl_4$ (125 μL, 0.01 M), and

https://doi.org/10.1021/acsnano.1c05970
ACS Nano 2021, 15, 19409−19417

thiosemicarbazide (TSC; 250 μL, 0.01 M). The resultant seed solution was stirred for 30 s and then left undisturbed at 35 °C for 2 h before further use. The growth solution was prepared through sequential addition of $HAuCl_4$ (2 mL, 0.01 M), $AgNO_3$ (400 μL, 0.01 M), HCl (800 μL, 1 M), and adipic acid (320 μL, 0.1 M) into an aqueous cetyltrimethylammonium bromide (CTAB) solution (40 mL, 0.1 M). The seed solution (50 μL) was then added into the growth solution, followed by inversion mixing for 5 s. The resultant solution was kept undisturbed at 35 °C for 6 h.

Purification of the Au NBPs. The as-prepared Au NBP solution (40 mL, longitudinal plasmon wavelength 950 nm, extinction value at the longitudinal plasmon peak 4) was centrifuged at 5500 rpm for 10 min and redispersed in a cetyltrimethylammonium chloride (CTAC) solution (30 mL, 0.08 M). $AgNO_3$ (8 mL, 0.01 M) and adipic acid (4 mL, 0.1 M) were subsequently added into the CTAC-stabilized Au NBP solution under gentle shaking. The resultant solution was kept at 60 °C for 6 h, during which Ag was deposited on the Au nanocrystals to produce bimetallic Au/Ag products. The Au/Ag products were then centrifuged at 5000 rpm for 10 min and redispersed in CTAB (30 mL, 0.05 M). The solution was left undisturbed at 35 °C overnight, during which the Au/Ag hetero-nanorods agglomerated and precipitated to the bottom of the container while the polyhedral Au/Ag nanoparticles remained in the supernatant. The Au/Ag hetero-nanorods were redispersed in DI water (20 mL) and subsequently mixed with $NH_3{\cdot}H_2O$ (400 μL, 30 wt %) and H_2O_2 (300 μL, 0.1 M) and kept for 4 h. During this process, the Ag segments were gradually etched away. The clear supernatant was carefully taken out. The resultant pure Au NBPs were separated by centrifugation (5500 rpm, 10 min) and redispersed in DI water for further use.

Experimental Setup. The linear and nonlinear response measurements were performed using a dark-field reflection microspectroscopy setup combined with a side-illumination component (see Figure S2). To study the linear properties, an incoherent white-light source (Energetiq Laser-Driven Light Source EQ-99) was utilized. With mirrors and an achromatic lens of 75 mm focal length, the white light was focused onto the sample with an incident angle of ~30°. The hybrid systems were imaged, and their scattering spectra were recorded based on a dark-field reflection setup consisting of a Nikon LV100 upright microscope combined with a grating monochromator (Princeton Instruments IsoPlane 160, 300 lines/mm, 500 nm blaze wavelengths) and a 2D Peltier-cooled CCD detector (Princeton Instruments PIXIS 256). To investigate the nonlinear behavior of the hybrid cavities, a mode-locked Ti:sapphire laser was employed as the excitation light source, which delivers 100 fs optical pulses at 80 MHz repetition rate and allows wavelength tunability in the range of 770−860 nm. A half wave plate was utilized to ensure that the illumination light is s-polarized (perpendicular to the plane of incidence and parallel to the lab table). By using a flip mirror in the side-illumination component, one can easily switch the illumination from the white light source to the laser source under the condition that the incident angle and focus conditions stay the same. A short-pass filter (FGB37, Thorlabs) is added before the detector to filter out the intensely scattered fundamental light. A Nikon TU Plan Fluor ELWD 60×, NA 0.7, objective is used for collecting scattered and emitted light under side illumination.

Power Calibration of the Spectrometer. Since the measured SHG signals are quite weak, it is very challenging to directly measure the corresponding SHG power. In order to estimate the SHG power from the intensity signal recorded by the spectrometer, we use the much stronger scattering signal of the fundamental mode and compare it to a power measurement carried out with a Si amplified detector (PDA36A2, Thorlabs). The Si detector is attached to the microscope as shown in Figure S2. The same signal is detected by the spectrometer through an intensity filter with a certain attenuation coefficient. The total number of counts per second, integrated over the full scattering peak width and corrected by the filter transmittance, is compared to the measured power, resulting in a value for the spectrometer efficiency at the laser center wavelength. The corresponding efficiency at the SHG wavelength is then estimated via the known spectral shape of the photodetector responsivity, the diffraction grating efficiency, and the CCD detector quantum yield. Finally, the total number of counts per second corresponding to the SHG signal is converted into a power value. For a typical SHG measurement, this yields a power on the order of picowatts. It should be mentioned that this value represents an average intensity and not a peak intensity.

ASSOCIATED CONTENT

Supporting Information

The Supporting Information is available free of charge at https://pubs.acs.org/doi/10.1021/acsnano.1c05970.

Measured scattering spectrum of an isolated bare gold nano-bipyramid on a silica substrate, schematic dark-field setup for white light scattering and nonlinear spectroscopy, Q-dependent second harmonic generation, nonlinear emission in Au NBPs on the fused silica substrate, double-log plot of excitation power dependence of SHG, and experimental excitation parameters and output power levels (PDF)

Dynamic nonlinear light from the gold NBPs on the tapered fiber with diameter 1.44 μm when the focus area of our excitation laser sweeps over the fiber (MOV)

AUTHOR INFORMATION

Corresponding Authors

Qi Ai − *4th Physics Institute and Research Center SCoPE, University of Stuttgart, 70569 Stuttgart, Germany;* orcid.org/0000-0002-1716-7638; Email: q.ai@pi4.uni-stuttgart.de

Harald Giessen − *4th Physics Institute and Research Center SCoPE, University of Stuttgart, 70569 Stuttgart, Germany;* Email: h.giessen@pi4.uni-stuttgart.de

Authors

Florian Sterl − *4th Physics Institute and Research Center SCoPE, University of Stuttgart, 70569 Stuttgart, Germany;* orcid.org/0000-0002-1025-6777

Han Zhang − *Department of Physics, The Chinese University of Hong Kong, Shatin, Hong Kong SAR, China*

Jianfang Wang − *Department of Physics, The Chinese University of Hong Kong, Shatin, Hong Kong SAR, China;* orcid.org/0000-0002-2467-8751

Complete contact information is available at: https://pubs.acs.org/10.1021/acsnano.1c05970

Author Contributions

H.G. and Q.A. designed the hybrid systems; Q.A. prepared the hybrid systems and carried out the experiments. Q.A. and F.S. performed the power calibration of the spectrometer. H.Z. and J.W. synthesized gold nano-bipyramid samples. Q.A. wrote the manuscript. All authors contributed to the discussions and the corrections of the manuscript.

Notes

The authors declare no competing financial interest.

ACKNOWLEDGMENTS

We thank Deutsche Forschungsgemeinschaft (GRK2642 PQE and SPP1839), Bundesministerium für Bildung und Forschung (BMBF), European Research Council (Advanced Grant ComplexPlas, PoC 3DPrintedOptics, Grant Agreement No. 862549), Ministerium für Forschung und Kunst Baden-Württemberg (IQST), Carl-Zeiss Stifutung, and Baden-

Württemberg Stiftung for funding. Q.A. acknowledges CSC for funding. The authors thank Mario Hentschel and Lili Gui for meaningful discussion, and Ksenia Weber for proofreading and helpful advice.

REFERENCES

(1) Simon, H. J.; Mitchell, D. E.; Watson, J. G. Optical Second-Harmonic Generation with Surface Plasmons in Silver Films. *Phys. Rev. Lett.* **1974**, *33*, 1531−1534.
(2) Maiuri, M.; Garavelli, M.; Cerullo, G. Ultrafast Spectroscopy: State of the Art and Open Challenges. *J. Am. Chem. Soc.* **2020**, *142*, 3−15.
(3) Huang, J. S.; Callegari, V.; Geisler, P.; Brüning, C.; Kern, J.; Prangsma, J. C.; Wu, X.; Feichtner, T.; Ziegler, J.; Weinmann, P.; Kamp, M.; Forchel, A.; Biagioni, P.; Sennhauser, U.; Hecht, B. Atomically Flat Single-Crystalline Gold Nanostructures for Plasmonic Nanocircuitry. *Nat. Commun.* **2010**, *1*, 150.
(4) Smolyaninov, I. I.; Zayats, A. V.; Davis, C. C. Near-Field Second Harmonic Generation from a Rough Metal Surface. *Phys. Rev. B: Condens. Matter Mater. Phys.* **1997**, *56*, 9290−9293.
(5) Bozhevolnyi, S. I.; Beermann, J.; Coello, V. Direct Observation of Localized Second-Harmonic Enhancement in Random Metal Nanostructures. *Phys. Rev. Lett.* **2003**, *90*, 197403.
(6) Lippitz, M.; Van Dijk, M. A.; Orrit, M. Third-Harmonic Generation from Single Gold Nanoparticles. *Nano Lett.* **2005**, *5*, 799−802.
(7) Russier-Antoine, I.; Benichou, E.; Bachelier, G.; Jonin, C.; Brevet, P. F. Multipolar Contributions of the Second Harmonic Generation from Silver and Gold Nanoparticles. *J. Phys. Chem. C* **2007**, *111*, 9044−9048.
(8) Hanke, T.; Krauss, G.; Träutlein, D.; Wild, B.; Bratschitsch, R.; Leitenstorfer, A. Efficient Nonlinear Light Emission of Single Gold Optical Antennas Driven by Few-Cycle Near-Infrared Pulses. *Phys. Rev. Lett.* **2009**, *103*, 257404.
(9) Butet, J.; Duboisset, J.; Bachelier, G.; Russier-Antoine, I.; Benichou, E.; Jonin, C.; Brevet, P. F. Optical Second Harmonic Generation of Single Metallic Nanoparticles Embedded in a Homogeneous Medium. *Nano Lett.* **2010**, *10*, 1717−1721.
(10) Kauranen, M.; Zayats, A. V. Nonlinear Plasmonics. *Nat. Photonics* **2012**, *6*, 737−748.
(11) Kravtsov, V.; Ulbricht, R.; Atkin, J. M.; Raschke, M. B. Plasmonic Nanofocused Four-Wave Mixing for Femtosecond near-Field Imaging. *Nat. Nanotechnol.* **2016**, *11*, 459−464.
(12) Rahmani, M.; Leo, G.; Brener, I.; Zayats, A. V.; Maier, S. A.; De Angelis, C.; Tan, H.; Flavio Gili, V.; Karouta, F.; Oulton, R.; Vora, K.; Lysevych, I.; Xu, L.; Miroshnichenko, A. E.; Jagadish, C.; Neshev, D. N.; Staude, M. Nonlinear Frequency Conversion in Optical Nanoantennas and Metasurfaces: Materials Evolution and Fabrication. *Opto-Electronic Adv.* **2018**, *1*, 18002101.
(13) Liu, S.; Sinclair, M. B.; Saravi, S.; Keeler, G. A.; Yang, Y.; Reno, J.; Peake, G. M.; Setzpfandt, F.; Staude, I.; Pertsch, T.; Brener, I. Resonantly Enhanced Second-Harmonic Generation Using III-V Semiconductor All-Dielectric Metasurfaces. *Nano Lett.* **2016**, *16*, 5426−5432.
(14) Ghirardini, L.; Carletti, L.; Gili, V.; Pellegrini, G.; Duò, L.; Finazzi, M.; Rocco, D.; Locatelli, A.; De Angelis, C.; Favero, I.; Ravaro, M.; Leo, G.; Lemaître, A.; Celebrano, M. Polarization Properties of Second-Harmonic Generation in AlGaAs Optical Nanoantennas. *Opt. Lett.* **2017**, *42*, 559.
(15) Vabishchevich, P. P.; Liu, S.; Sinclair, M. B.; Keeler, G. A.; Peake, G. M.; Brener, I. Enhanced Second-Harmonic Generation Using Broken Symmetry III-V Semiconductor Fano Metasurfaces. *ACS Photonics* **2018**, *5*, 1685−1690.
(16) Lehr, D.; Reinhold, J.; Thiele, I.; Hartung, H.; Dietrich, K.; Menzel, C.; Pertsch, T.; Kley, E. B.; Tünnermann, A. Enhancing Second Harmonic Generation in Gold Nanoring Resonators Filled with Lithium Niobate. *Nano Lett.* **2015**, *15*, 1025−1030.
(17) Pu, Y.; Grange, R.; Hsieh, C. L.; Psaltis, D. Nonlinear Optical Properties of Core-Shell Nanocavities for Enhanced Second-Harmonic Generation. *Phys. Rev. Lett.* **2010**, *104*, 207402.
(18) Valev, V. K.; Silhanek, A. V.; Verellen, N.; Gillijns, W.; Van Dorpe, P.; Aktsipetrov, O. A.; Vandenbosch, G. A. E.; Moshchalkov, V. V.; Verbiest, T. Asymmetric Optical Second-Harmonic Generation from Chiral G-Shaped Gold Nanostructures. *Phys. Rev. Lett.* **2010**, *104*, 127401.
(19) Belardini, A.; Larciprete, M. C.; Centini, M.; Fazio, E.; Sibilia, C.; Chiappe, D.; Martella, C.; Toma, A.; Giordano, M.; Buatier De Mongeot, F. Circular Dichroism in the Optical Second-Harmonic Emission of Curved Gold Metal Nanowires. *Phys. Rev. Lett.* **2011**, *107*, 257401.
(20) Ahmadivand, A.; Semmlinger, M.; Dong, L.; Gerislioglu, B.; Nordlander, P.; Halas, N. J. Toroidal Dipole-Enhanced Third Harmonic Generation of Deep Ultraviolet Light Using Plasmonic Meta-Atoms. *Nano Lett.* **2019**, *19*, 605−611.
(21) Genevet, P.; Tetienne, J. P.; Gatzogiannis, E.; Blanchard, R.; Kats, M. A.; Scully, M. O.; Capasso, F. Large Enhancement of Nonlinear Optical Phenomena by Plasmonic Nanocavity Gratings. *Nano Lett.* **2010**, *10*, 4880−4883.
(22) Thyagarajan, K.; Butet, J.; Martin, O. J. F. Augmenting Second Harmonic Generation Using Fano Resonances in Plasmonic Systems. *Nano Lett.* **2013**, *13*, 1847−1851.
(23) Lee, J.; Tymchenko, M.; Argyropoulos, C.; Chen, P.-Y.; Lu, F.; Demmerle, F.; Boehm, G.; Amann, M.-C.; Alù, A.; Belkin, M. A. Giant Nonlinear Response from Plasmonic Metasurfaces Coupled to Intersubband Transitions. *Nature* **2014**, *511*, 65−69.
(24) Butet, J.; Dutta-Gupta, S.; Martin, O. J. F. Surface Second-Harmonic Generation from Coupled Spherical Plasmonic Nanoparticles: Eigenmode Analysis and Symmetry Properties. *Phys. Rev. B: Condens. Matter Mater. Phys.* **2014**, *89*, 245449.
(25) Czaplicki, R.; Kiviniemi, A.; Huttunen, M. J.; Zang, X.; Stolt, T.; Vartiainen, I.; Butet, J.; Kuittinen, M.; Martin, O. J. F.; Kauranen, M. Less Is More: Enhancement of Second-Harmonic Generation from Metasurfaces by Reduced Nanoparticle Density. *Nano Lett.* **2018**, *18*, 7709−7714.
(26) Hentschel, M.; Utikal, T.; Giessen, H.; Lippitz, M. Quantitative Modeling of the Third Harmonic Emission Spectrum of Plasmonic Nanoantennas. *Nano Lett.* **2012**, *12*, 3778−3782.
(27) Metzger, B.; Hentschel, M.; Lippitz, M.; Giessen, H. Third-Harmonic Spectroscopy and Modeling of the Nonlinear Response of Plasmonic Nanoantennas. *Opt. Lett.* **2012**, *37*, 4741.
(28) Aouani, H.; Navarro-Cia, M.; Rahmani, M.; Sidiropoulos, T. P. H.; Hong, M.; Oulton, R. F.; Maier, S. A. Multiresonant Broadband Optical Antennas as Efficient Tunable Nanosources of Second Harmonic Light. *Nano Lett.* **2012**, *12*, 4997−5002.
(29) Thyagarajan, K.; Rivier, S.; Lovera, A.; Martin, O. J. F. Enhanced Second-Harmonic Generation from Double Resonant Plasmonic Antennae. *Opt. Express* **2012**, *20*, 12860.
(30) Celebrano, M.; Wu, X.; Baselli, M.; Großmann, S.; Biagioni, P.; Locatelli, A.; De Angelis, C.; Cerullo, G.; Osellame, R.; Hecht, B.; Duò, L.; Ciccacci, F.; Finazzi, M. Mode Matching in Multiresonant Plasmonic Nanoantennas for Enhanced Second Harmonic Generation. *Nat. Nanotechnol.* **2015**, *10*, 412−417.
(31) Liu, S. D.; Leong, E. S. P.; Li, G. C.; Hou, Y.; Deng, J.; Teng, J. H.; Ong, H. C.; Lei, D. Y. Polarization-Independent Multiple Fano Resonances in Plasmonic Nonamers for Multimode-Matching Enhanced Multiband Second-Harmonic Generation. *ACS Nano* **2016**, *10*, 1442−1453.
(32) Yang, K. Y.; Butet, J.; Yan, C.; Bernasconi, G. D.; Martin, O. J. F. Enhancement Mechanisms of the Second Harmonic Generation from Double Resonant Aluminum Nanostructures. *ACS Photonics* **2017**, *4*, 1522−1530.
(33) Zou, S.; Janel, N.; Schatz, G. C. Silver Nanoparticle Array Structures That Produce Remarkably Narrow Plasmon Lineshapes. *J. Chem. Phys.* **2004**, *120*, 10871−10875.
(34) Auguié, B.; Barnes, W. L. Collective Resonances in Gold Nanoparticle Arrays. *Phys. Rev. Lett.* **2008**, *101*, 143902.

https://doi.org/10.1021/acsnano.1c05970
ACS Nano 2021, 15, 19409−19417

(35) Grinblat, G.; Rahmani, M.; Cortés, E.; Caldarola, M.; Comedi, D.; Maier, S. A.; Bragas, A. V. High-Efficiency Second Harmonic Generation from a Single Hybrid ZnO Nanowire/Au Plasmonic Nano-Oligomer. *Nano Lett.* **2014**, *14*, 6660−6665.
(36) Taubert, R.; Hentschel, M.; Kästel, J.; Giessen, H. Classical Analog of Electromagnetically Induced Absorption in Plasmonics. *Nano Lett.* **2012**, *12*, 1367−1371.
(37) Floess, D.; Hentschel, M.; Weiss, T.; Habermeier, H. U.; Jiao, J.; Tikhodeev, S. G.; Giessen, H. Plasmonic Analog of Electromagnetically Induced Absorption Leads to Giant Thin Film Faraday Rotation of 14°. *Phys. Rev. X* **2017**, *7*, 021048.
(38) Huttunen, M. J.; Reshef, O.; Stolt, T.; Dolgaleva, K.; Boyd, R. W.; Kauranen, M. Efficient Nonlinear Metasurfaces by Using Multiresonant High-Q Plasmonic Arrays. *J. Opt. Soc. Am. B* **2019**, *36*, E30.
(39) Suhailin, F. H.; Alwahib, A. A.; Kamil, Y. M.; Abu Bakar, M. H.; Huang, N. M.; Mahdi, M. A. Fiber-Based Surface Plasmon Resonance Sensor for Lead Ion Detection in Aqueous Solution. *Plasmonics* **2020**, *15*, 1369−1376.
(40) Miliutina, E.; Kalachyova, Y.; Postnikov, P.; Švorčík, V.; Lyutakov, O. Enhancement of Surface Plasmon Fiber Sensor Sensitivity through the Grafting of Gold Nanoparticles. *Photonic Sens.* **2020**, *10*, 105−112.
(41) Lee, S.; Song, H.; Ahn, H.; Kim, S.; Choi, J.-r.; Kim, K. Fiber-Optic Localized Surface Plasmon Resonance Sensors Based on Nanomaterials. *Sensors* **2021**, *21*, 819.
(42) Ai, Q.; Gui, L.; Paone, D.; Metzger, B.; Mayer, M.; Weber, K.; Fery, A.; Giessen, H. Ultranarrow Second-Harmonic Resonances in Hybrid Plasmon-Fiber Cavities. *Nano Lett.* **2018**, *18*, 5576−5582.
(43) Fang, C.; Zhao, G.; Xiao, Y.; Zhao, J.; Zhang, Z.; Geng, B. Facile Growth of High-Yield Gold Nanobipyramids Induced by Chloroplatinic Acid for High Refractive Index Sensing Properties. *Sci. Rep.* **2016**, *6*, 36706.
(44) Pricking, S.; Giessen, H. Tapering Fibers with Complex Shape. *Opt. Express* **2010**, *18*, 3426.
(45) Wang, P.; Wang, Y.; Yang, Z.; Guo, X.; Lin, X.; Yu, X. C.; Xiao, Y. F.; Fang, W.; Zhang, L.; Lu, G.; Gong, Q.; Tong, L. Single-Band 2-Nm-Line-Width Plasmon Resonance in a Strongly Coupled Au Nanorod. *Nano Lett.* **2015**, *15*, 7581−7586.
(46) Linden, S.; Niesler, F. B. P.; Förstner, J.; Grynko, Y.; Meier, T.; Wegener, M. Collective Effects in Second-Harmonic Generation from Split-Ring-Resonator Arrays. *Phys. Rev. Lett.* **2012**, *109*, 015502.
(47) Hanke, T.; Cesar, J.; Knittel, V.; Trügler, A.; Hohenester, U.; Leitenstorfer, A.; Bratschitsch, R. Tailoring Spatiotemporal Light Confinement in Single Plasmonic Nanoantennas. *Nano Lett.* **2012**, *12*, 992−996.
(48) Wang, F.; Harutyunyan, H. Tailoring the Quality Factors and Nonlinear Response in Hybrid Plasmonic-Dielectric Metasurfaces. *Opt. Express* **2018**, *26*, 120.
(49) Ai, Q.; Zhang, H.; Wang, J.; Giessen, H. Multiphoton Photoluminescence in Hybrid Plasmon-Fiber Cavities with Au and Au@Pd Nanobipyramids: Two-Photon *versus* Four-Photon Processes and Rapid Quenching. *ACS Photonics* **2021**, *8*, 2088−2094.
(50) Shcherbakov, M. R.; Werner, K.; Fan, Z.; Talisa, N.; Chowdhury, E.; Shvets, G. Photon Acceleration and Tunable Broadband Harmonics Generation in Nonlinear Time-Dependent Metasurfaces. *Nat. Commun.* **2019**, *10*, 1345.
(51) Ren, M.-L.; Liu, W.; Aspetti, C. O.; Sun, L.; Agarwal, R. Enhanced Second-Harmonic Generation from Metal-Integrated Semiconductor Nanowires *via* Highly Confined Whispering Gallery Modes. *Nat. Commun.* **2014**, *5*, 5432.
(52) Gui, L.; Bagheri, S.; Strohfeldt, N.; Hentschel, M.; Zgrabik, C. M.; Metzger, B.; Linnenbank, H.; Hu, E. L.; Giessen, H. Nonlinear Refractory Plasmonics with Titanium Nitride Nanoantennas. *Nano Lett.* **2016**, *16*, 5708−5713.
(53) Liu, M.; Guyot-Sionnest, P. Mechanism of Silver(I)-Assisted Growth of Gold Nanorods and Bipyramids. *J. Phys. Chem. B* **2005**, *109*, 22192−22200.
(54) Kou, X.; Zhang, S.; Tsung, C. K.; Yeung, M. H.; Shi, Q.; Stucky, G. D.; Sun, L.; Wang, J.; Yan, C. Growth of Gold Nanorods and Bipyramids Using CTEAB Surfactant. *J. Phys. Chem. B* **2006**, *110*, 16377−16383.
(55) Kou, X.; Ni, W.; Tsung, C. K.; Chan, K.; Lin, H. Q.; Stucky, G. D.; Wang, J. Growth of Gold Bipyramids with Improved Yield and Their Curvature-Directed Oxidation. *Small* **2007**, *3*, 2103−2113.

https://doi.org/10.1021/acsnano.1c05970
ACS Nano 2021, 15, 19409−19417